Multi-failure theory of composite orthogrid sandwich cylinder

Shu Jiang [a, b], Fangfang Sun [a, *], Hualin Fan [a, *]

[a] *Research center of Lightweight Structures and Intelligent Manufacturing, State Key Laboratory of Mechanics and Control of Mechanical Structures, Nanjing University of Aeronautics and Astronautics, Nanjing 210016, China*

[b] *College of Mechanics and Materials, Hohai University, Nanjing 210098, China*

**Corresponding Authors*: fhl15@nuaa.edu.cn(Fan HL); sunff1986@163.com(Sun FF)

Abstract: Weight-efficient carbon fiber reinforced composite (CFRC) anisogrid structures gained a lot of attention in recent years. Under uniaxial compression, CFRC orthogrid-core sandwich cylinder has four potential failure modes, including global buckling, facesheet mono-cell buckling, orthogrid rib buckling and material failure. A smearing method was proposed to predict the equivalent stiffness of the structure and calculate the stress state of the facesheets and the orthogrid, providing fundaments to build the failure criteria. Analytical studies and theoretical models were carried out to reveal the failure modes and predict the load capacity of the CFRC orthogrid cylinder under axial compression by the way of failure maps, which provides a convenient and reliable method for the optimal design of the CFRC anisogrid cylinder.

Key words: composite structure; carbon fiber; theoretical prediction

1 Introduction

Recently, composite lattice structures gained more and more attention for its advantage of weight efficiency, high specific strength and specific stiffness [1-3]. Among them, CFRC anisogrid structures [4-9] have been applied in rockets, satellites,

launch vehicles and airplanes. Usually the structural concept considered for a spacecraft body structure is an anisogrid stiffened skin with a laminate configuration and the stiffener grid geometry is selected to the best suit for design requirements [4].

Fan et al. [10-16] developed CFRC anisogrid lattice-core sandwich shells and they found the sandwich style endow the cylinder greater stiffness and strength compared with stiffened cylinder [4] through restricting rib buckling [10]. Hu et al. [17] designed and fabricated corrugated lattice truss composite sandwich pane. The lattice core is made up of orthogonal corrugated lattice trusses and this structure was applied to construct CFRC lattice truss sandwich cylinder by Li et al. [17]. Yang et al. [18] developed all-composite corrugated sandwich cylindrical shells.

Under uniaxial compression, CFRC anisogrid-core sandwich cylinder usually has four potential failure modes, including global buckling, facesheet mono-cell buckling, rib buckling and material failure [10, 19]. A smearing method was proposed to predict the equivalent stiffness of the Isogrid sandwich structure [10, 19]. Fan et al. [10] and Sun et al. [19] build multi-failure criteria of CFRC Isogrid sandwich cylinder.

In this paper, a smearing method and multi-failure criteria were developed to analyze the mechanical behaviors of CFRC orthogrid-core sandwich cylinder.

2 Failure modes

A new type of carbon fiber orthogrid-core sandwich cylinder was designed and fabricated by interlocking and filament winding technique [20], as shown in Fig. 1. The diameter of the cylinder, D, is 625 mm, and the height, H, is 392.7 mm. Skin thickness of the cylinder is 1.0 mm. The height of the grid core, c, is 8 mm. Rib

thickness and width of the orthogrid are 2.0 mm and 8.0 mm, respectively. T700/epoxy-resin carbon fibers were used to manufacture the cylinder by hot-pressing technology. Through uniaxial compression test of the cylinder, the failure load is 302.75 kN. At the top of the cylinder, the facesheet failed at laminate delamination, and then induced debonding and wrinkling in post-failure stage, as shown in Fig.1. In the test, material failure controls the ultimate load of the cylinder.

Changing the geometrical dimensions of the cylinder, three typical instabilities are acquired through finite element modeling (FEM), as shown in Fig. 2. When the sandwich wall is thin enough, the sandwich cylinder fails at global buckling. When the skin is thin enough, mono-cell buckling is found. When the rib of the orthogrid is thin enough, the cylinder fails at rib buckling.

2 Theoretical analyses

2.1 Equivalent theory

According to the conversion relationship between axial force and deformation in all directions and the stress and strain of the equivalent homogeneous element, a single element of rectangular grid structure can be equivalent to continuum, as shown in Fig. 3. The equivalent elastic modulus, E, of the orthogrid is given by

$$E = \frac{E_{r1} t_r}{h}, \tag{1}$$

where E_{r1} is the elastic modulus of grid. t_r and h are the thickness of the rib and the length of the unit orthogrid cell. It puts forward that the skin and grid are equivalent to homogeneous structure respectively, then, according to the principle of equivalent that tensile stiffness and bending stiffness are invariable, the sandwich

structure is equivalent to a homogeneous panel or shell structure, which needs the equivalent elastic modulus, E_e, and equivalent thickness, t_e, of the structure, but both of them are unknown quantities. For the convenience of calculation, it is necessary to define the parameters as follows: E_{s1} and E_{s2} are elastic modulus of external and inner skin; E_{r1} is elastic modulus of the orthogrid rib; t_1 and t_2 are thickness of outer and inner skin; t_r and d_r are the width and height of the orthogrid; E_1^* and E_2^* are elastic modulus of two skins of sandwich and E_r^* is elastic modulus of sandwich core, as shown in Fig. 3. Defining the relative density of the orthogrid, $\rho^* = 2t_r / h$; the effective thickness of the orthogrid panel, $b = t_r E_{r1} / E_{s1}$; the thickness ratio of the inner and the external skin, $\lambda = t_2 / t_1$; the ratio of the height of orthogrid and the thickness of external skin, $\delta = d_r / t_1$; the ratio of elastic modulus of the orthogrid and the external skin, $\eta = E_{r1} / E_{s1}$; the ratio of elastic modulus of inner and external skin, $\xi = E_{s2} / E_{s1}$, the in-plane effective elastic modulus of the orthogrid is $E_r^* = \rho^* E_{r1} / 2 = E_{r1} t_r / h$; the ratio of the equivalent tensile stiffness of the core layer and the external skin is $\alpha = \rho^* \eta \delta / 2$; the ratio of the equivalent tensile stiffness of the inner and the external skins is $\mu = \lambda \xi$.

Equivalent homogenization of the sandwich structure is based on rectangular grid structure, which is a two-dimensional isotropic panel. In smearing process, the orthogrid-core sandwich turns to a sandwich structure, and then turns to the equivalent homogeneous solid shell, as shown in Fig. 3. Since the skin itself is a homogeneous continuous structure, so that $E_1^* = E_{s1}$, $E_2^* = E_{s2}$ and $E_2^* = E_{s2}$. The equivalent tensile stiffness, K_e, is

$$K_e = \left(E_1^* t_1 + E_r^* d_r + E_2^* t_2\right) / \left(1\text{-}v^2\right). \tag{2}$$

The equivalent bending stiffness, D_e, is given by:

$$D_e = \frac{E_1^* t_1^3}{12(1-v^2)} + E_1^* t_1 \left(y_1 - \bar{y}\right)^2 + \frac{E_r^* d_r^3}{12(1-v^2)} + E_r^* d_r \left(y_2 - \bar{y}\right)^2 + \frac{E_2^* t_2^3}{12(1-v^2)} + E_2^* t_2 \left(y_3 - \bar{y}\right)^2, \tag{3}$$

where $\bar{y}$ is the neutral axis section of the sandwich structure and calculated by

$$E_1^* t_1 \left(y_1 - \bar{y}\right) + E_r^* d_r \left(y_2 - \bar{y}\right) + E_2^* t_2 \left(y_3 - \bar{y}\right) = 0. \tag{4}$$

Respectively, y_1, y_2 and y_3 are the ordinates of the center of the rectangular cross section of three laminates and given by

$$y_1 = t_1 \left(1/2 + \lambda + \delta\right), \quad y_2 = t_1 \left(\lambda + \delta/2\right), y_3 = \lambda t_1 / 2. \tag{5}$$

Then D_e is given by

$$D_e = \frac{\beta^2 E_{s1} t_1^3}{12(1-v^2)(1+\alpha+\mu)}, \tag{6}$$

$$\beta^2 = 3\mu\left(\delta+\lambda\right)^2 + 3\left(1+\delta\right)^2 + 1 + \alpha\delta^2 + \mu\lambda^2 - 3\left[1+\delta-\mu\left(\delta+\lambda\right)\right]^2. \tag{7}$$

According to the principle of equal tensile and bending stiffness, the equivalent modulus, E_e, and the equivalent thickness, t_e, can be achieved. The equivalent tensile stiffness, K_e, of homogeneous panel is $K_e = E_e t_e / \left(1-v^2\right)$. D_e is simplified to $D_e = E_e t_e^3 / \left[12(1-v^2)\right]$. The equivalent modulus and thickness are given by

$$E_e = \left(1+\alpha+\mu\right)^2 E_{s1} / \beta, \quad t_e = t_1 \beta / \left(1+\alpha+\mu\right). \tag{8}$$

In addition, under the action of external force, the relationship between the internal force of the skin and grid of the grid sandwich structure must be given, as shown in Fig. 4. The stresses of the external skin and the inner skin are calculated by

$$\begin{Bmatrix} \sigma_x \\ \sigma_y \\ \tau_{xy} \end{Bmatrix} = \frac{1}{t_1\left(1+\alpha+\mu\right)} \begin{Bmatrix} N_x \\ N_y \\ N_{xy} \end{Bmatrix}, \quad \begin{Bmatrix} \sigma_x \\ \sigma_y \\ \tau_{xy} \end{Bmatrix} = \frac{\xi}{t_1\left(1+\alpha+\mu\right)} \begin{Bmatrix} N_x \\ N_y \\ N_{xy} \end{Bmatrix}. \tag{9}$$

3 Failure modes

3.1 Global buckling

The global buckling analysis is making orthogrid-core sandwich cylinder be equivalent to a thin homogeneous cylinder in axial compression. The buckling mode is curve and bending in the middle of cylinder and the buckling wavelength is the height of cylinder, as shown in Fig. 5. Under the assumption of small deformation, the small deflection differential equation is given by

$$D_e \nabla^8 w + \frac{Et}{R^2}\frac{\partial^4 w}{\partial x^4} + \nabla^4 (N_x \frac{\partial^2 w}{\partial x^2} + 2N_{xy}\frac{\partial^2 w}{\partial x \partial y} + N_y \frac{\partial^2 w}{\partial y^2}) = 0 , \tag{10}$$

where N_x, N_y and N_{xy} are longitudinal tensile stress, circumferential tensile stress and shear stress respectively; w is normal deflection; $R = D/2$. If the cylinder is only subjected to axial force, Eq. (10) can be simplified to

$$D_e \nabla^8 w + \frac{Et}{R^2}\frac{\partial^4 w}{\partial x^4} + \frac{P}{2\pi R}\nabla^4 \frac{\partial^2 w}{\partial x^2} = 0 . \tag{11}$$

For thin cylindrical shells being axially compressed, there are two types of buckling and they are divided into symmetric and asymmetric buckling. For symmetric buckling under the simple support boundary condition, the deflection function is:

$$w(x) = \sum_{m=1}^{\infty} A_m \sin\left(m\pi x / H\right), \tag{12}$$

where m is the number of half wave along the axial direction of the cylindrical buckling, and A_m is a constant. Putting deflection into Eq. (12), it is obtained that

$$\sum_{m=1}^{\infty} A_m \left[D_e \left(\frac{m\pi}{H}\right)^8 - \frac{P}{2\pi R}\left(\frac{m\pi}{H}\right)^6 + \frac{E_e t_e}{R^2}\left(\frac{m\pi}{H}\right)^4 \right] \sin\frac{m\pi x}{H} = 0 . \tag{13}$$

The buckling critical load is given by

$$P_{cr} = \frac{2\gamma\pi}{\sqrt{3(1-v^2)}} \frac{E_e t_e^2}{R}, \tag{14}$$

where geometric parameter $\gamma = \frac{1}{2}\left(\frac{\pi^2}{Z\sqrt{12}} m^2 + \frac{Z\sqrt{12}}{\pi^2} \frac{1}{m^2} \right)$ and $Z = \frac{H^2\sqrt{1-v^2}}{Rt}$.

Since the minimum value of γ is 1, the minimum value of the critical load is

$$P_{cr} = 2\pi E_e t_e^2 / \left(R\sqrt{3(1-v^2)} \right). \tag{15}$$

For asymmetric buckling under simply-supported boundary conditions, the deflection function is given by

$$w(x) = \sum_{m=1}^{\infty}\sum_{n=1}^{\infty} A_{mn} \sin\left(m\pi x / H\right) \sin\left(ny / R\right), \tag{16}$$

where n is the number of half wave along the circular direction and A_{mn} is a constant. Making $\beta = nH / \left(\pi R\right)$, it can be obtained that

$$D_e \left(\frac{(m^2+\beta^2)\pi}{H} \right)^4 - \frac{P_{cr}}{2\pi R} \left(\frac{m\pi(m^2+\beta^2)}{H} \right)^2 + \frac{E_e t_e}{R^2} m^4 = 0. \tag{17}$$

Critical buckling load is obtained by

$$P_{cr} = \frac{2D_e \pi^3 R}{H^2} \frac{(m^2+\beta^2)^2}{m^2} + \frac{E_e t_e h^2}{\pi^2 R^2} \frac{m^2}{(m^2+\beta^2)^2}, \tag{18}$$

and the minimum value of the critical load is

$$P_{cr} = \frac{K_c \pi^3 R E_e}{6(1-v^2)} \frac{t_e^3}{H^2}, \tag{19}$$

where $K_c = P_{cr} H^2 / \left(2D_e \pi^3 R\right)$ and geometric parameter $Z = H^2\sqrt{1-v^2} / \left(Rt_e\right)$.

When K_c comes to the minimum, it can lead to the following formula as

$$\frac{(m^2+\beta^2)^2}{m^2} = \frac{12Z^2}{\pi^4} \frac{m^2}{(m^2+\beta^2)^2}. \tag{20}$$

with $\beta = \sqrt{m\left(\sqrt{2\sqrt{3}Z} / \pi - m\right)}$. If β has a real solution, $Z \geq \pi^2 m^2 / 2\sqrt{3}$. In this

paper, $Z \geq 2.85$, K_c has minimum value and the minimum critical buckling load is:

$$P_{cr} = 2\pi E_e t_e^2 / \sqrt{3(1-v^2)} . \tag{21}$$

The buckling load of the rectangular lattice sandwich cylinder is simplified as

$$P_{cr1} = 2\pi\gamma\beta E_1 t_1^{\ 2} / \sqrt{3(1-v^2)} . \tag{22}$$

3.3 Skin wrinkling

The wrinkling of the skin can be considered as the buckling of the short cylinder whose thickness is t_1, as shown in Fig. 5, and the height is h, the spacing between two orthogrid ribs. The differential equation of the cylinder which is given by

$$D_s \nabla^8 w + \frac{E_s t_1}{R^2}\frac{\partial^4 w}{\partial x^4} + \nabla^4\left(N_x \frac{\partial^2 w}{\partial x^2} + 2N_{xy}\frac{\partial^2 w}{\partial x \partial y} + N_y \frac{\partial^2 w}{\partial y^2}\right) = 0, \tag{23}$$

where D_s is bending stiffness of skin, $D_s = E_s t_1^{\ 3} / \left[12(1-v^2)\right]$; E_s is elastic modulus of skin; t_1 is thickness of skin; N_x, N_y and N_{xy} are longitudinal tensile stress, circumferential tensile stress and shear stress.

The load acting on the cylinder is considered as a force distributed uniformly along the thickness, the buckling load of the monocell buckling, P_{crs2}, is

$$P_{crs2} = \frac{K_c \pi^3 R E_{s1}}{6(1-v^2)}\frac{t_1^{\ 2}}{h^2} . \tag{24}$$

On the basis of the axial deformation of the skin and the sandwich are equal, the load is in direct proportion to the stiffness. Then, the buckling load, P_{cr2}, is given by

$$P_{cr2} = E_{s1}(1+\alpha+\mu)\frac{K_c \pi^3 R}{6(1\text{-}v^2)}\frac{t_1^{\ 2}}{h^2}, \tag{25}$$

with $K_c = \frac{(m^2+b^2)^2}{m^2} + \frac{12Z^2}{\pi^4}\frac{m^2}{(m^2+b^2)^2}$. According to the suggestion in reference [10, 19], $K_c = 11.0$. Z is geometrical parameter and $Z = h^2\sqrt{1-v^2} / \left(Rt_1\right)$.

3.4 Orthogrid rib buckling

Orthogrid rib buckling can be simplified as instability of a rectangular orthotropic panel with simple support, as shown in Fig. 5. Uniform pressure along the length is N_x. From the analysis of plane plate theory, the stresses are respectively given by

$$\sigma_x = -N_x / t_r, \sigma_y = 0, \tau_{xy} = 0 \quad . \tag{26}$$

The bending differential equation of anisotropic panel can be expressed by

$$\left(D_1 \frac{\partial^4}{\partial x^4} + D_2 \frac{\partial^4}{\partial y^4} + 2D_3 \frac{\partial^4}{\partial x^2 y^2} \right) w + N_x \frac{\partial^2 w}{\partial x^2} = 0, \tag{27}$$

where D_1 and D_2 are rib bending stiffness and D_k is the torsional stiffness. $D_1 = E_{r1} t_r^3 / \left[12(1-v_1 v_2)\right]$, $D_2 = E_{r2} t_r^3 / \left[12(1-v_1 v_2)\right]$, $D_k = G_{r12} t_r^3 / 12$ and $D_3 = v_2 D_1 + 2D_k = v_1 D_2 + 2D_k$. E_{r1} and E_{r2} are elastic modulus of orthogrid ribs in two directions, respectively. G_{r12} is in-plane shear modulus of orthogrid ribs, v_1, v_2 are the Poisson's ratio of the orthogrid rib in two directions, $v_1 E_{r1} = v_2 E_{r2}$. For simply supported ribs, the deflection is assumed as

$$w = \sum_{m=1}^{\infty} \sum_{n=1}^{\infty} A_{mn} \sin \frac{m\pi x}{h} \sin \frac{n\pi y}{d_r} . \tag{28}$$

When the longitudinal load, N_x, is very small and taking arbitrary values of m and n, the value in the brackets is greater than zero. So, the coefficient A_{mn} must be equal to zero, and the sheet is in equilibrium. When the longitudinal load exceeds the critical value, the sheet is bent, so that the critical value of the longitudinal load should satisfy the following condition:

$$D_1 \left(\frac{m\pi}{h} \right)^4 + D_2 \left(\frac{n\pi}{d_r} \right)^4 + 2D_3 \left(\frac{m\pi}{h} \right)^2 \left(\frac{n\pi}{d_r} \right)^2 - N_x \left(\frac{m\pi}{h} \right)^2 = 0 . \tag{29}$$

Since N_x is increased with the increase of n, n should be taken as 1. Then

$$N_x = \pi^2 h^2 \left[\frac{D_1 m^2}{h^4} + \frac{D_2}{d_r{}^4 m^2} + \frac{2D_3}{h^2 d_r{}^2} \right]. \tag{30}$$

Therefore, the critical stress can be obtained as

$$\sigma_{cr} = 2\pi^2 \left(\sqrt{D_1 D_2} + D_3 \right) / \left(d_r{}^2 t_r \right). \tag{31}$$

The relationship between the rib stress and the axial load of the cylinder is given by

$$\sigma_{cr} = \frac{E_r^*}{E_1^* t_1 \left(1+\alpha+\mu\right)} \frac{P_{cr3}}{2N_c t_r}. \tag{32}$$

Therefore, the critical load of the cylinder controlled by the rib buckling is

$$P_{cr3} = \frac{4\pi^2 t_1 h N_c (1+\alpha+\mu)}{\eta t_r} \left(\frac{\sqrt{D_1 D_2} + D_3}{d_r{}^2} \right). \tag{33}$$

3.5 Material failure

The strength of the skin applies Hill-Tsai formula for the calculation, and the main consideration is the stress of the layer in $\pm 45°$ directions, as shown in Fig. 5. When the cylinder is subjected to axial pressure, then $N_x = 0$ and $N_{xy} = 0$, thus $\sigma_x = 0$, $\sigma_y = N_y / \left[t_1 \left(1+\alpha+\mu\right) \right]$ and $\tau_{xy} = 0$. The global strain of the skin is given by

$$\begin{Bmatrix} \varepsilon_x \\ \varepsilon_y \\ \gamma_{xy} \end{Bmatrix} = \frac{1}{E_{s1} t_1 \left(1+\alpha+\mu\right)} \begin{bmatrix} 1 & -\nu & 0 \\ -\nu & 1 & 0 \\ 0 & 0 & 2(1+\nu) \end{bmatrix} \begin{Bmatrix} N_x \\ N_y \\ N_{xy} \end{Bmatrix}. \tag{34}$$

When $\nu = 1/3$, strains and stresses in $\pm 45°$ directions are. Stresses in $\pm 45°$ directions of skin are given by

$$\begin{Bmatrix} \varepsilon_1 \\ \varepsilon_2 \\ \gamma_{12} \end{Bmatrix} = \frac{\sigma_y}{E_{s1}} \begin{Bmatrix} 1/3 \\ 1/3 \\ 4/3 \end{Bmatrix}, \quad \begin{Bmatrix} \sigma_1 \\ \sigma_2 \\ \tau_{12} \end{Bmatrix} = \begin{bmatrix} E_{r1} & E_{r12} & 0 \\ E_{r21} & E_{r2} & 0 \\ 0 & 0 & G_{r12} \end{bmatrix} \begin{Bmatrix} \sigma_y / \left(3E_{s1}\right) \\ \sigma_y / \left(3E_{s1}\right) \\ 4\sigma_y / \left(3E_{s1}\right) \end{Bmatrix}. \tag{35}$$

With $E_{r12} = \nu_{21} E_{r2}$, $E_{r21} = \nu_{12} E_{r1}$, $E_{r21} = E_{r12}$ and $\nu_{21} = 1/3$. Then

$$\sigma_1 = \frac{1}{3} \frac{E_{r1}}{E_{s1}} \sigma_y + \frac{1}{9} \frac{E_{r2}}{E_{s1}} \sigma_y, \quad \sigma_2 = \frac{4}{9} \frac{E_{r2}}{E_{s1}} \sigma_y, \quad \tau_{12} = \frac{4}{3} \frac{G_{r12}}{E_{s1}} \sigma_y. \tag{36}$$

Stresses of skin, σ_1, σ_2 and τ_{12}, should satisfy the Hill-Tsai criterion, i.e.:

$$\frac{\sigma_1^{\ 2}}{X^2}-\frac{\sigma_1\sigma_2}{X^2}+\frac{\sigma_2^{\ 2}}{Y^2}+\frac{\tau_{12}^{\ 2}}{S^2}\le 1, \tag{37}$$

where X and Y are the ultimate strength of the fiber in the direction of $0°$ and $90°$, and S is the shear strength . The stress value is substituted into Eq. (46), i.e.:

$$\sigma_y \le E_{s1}\left[\frac{1}{X^2}\left(\frac{1}{9}E_{r1}^2-\frac{2}{27}E_{r1}E_{r2}-\frac{1}{27}E_{r2}^2\right)+\frac{1}{Y^2}\left(\frac{4}{9}E_{r2}\right)^2+\frac{1}{S^2}\left(\frac{4}{3}G_{r12}\right)^2\right]^{-\frac{1}{2}}. \tag{38}$$

Therefore, the critical load to satisfy the strength condition is given by

$$P_{cr4}=2\pi Rt_1(1+\alpha+\mu)E_{s1}\left[\left(\frac{1}{9}\frac{E_{r1}^2}{X^2}-\frac{2}{27}\frac{E_{r1}E_{r2}}{X^2}-\frac{1}{27}\frac{E_{r2}^2}{X^2}\right)+\left(\frac{4}{9}\frac{E_{r2}}{Y^2}\right)^2+\left(\frac{4}{3}\frac{G_{r12}}{S}\right)^2\right]^{-\frac{1}{2}}. \tag{39}$$

4 Failure prediction and failure maps

The orthogrid-core sandwich cylinder's failure mode is complex, so it's necessary to find the failure modes changed with the geometric parameters. The regimes of failure modes can be illustrated in failure maps, which are assumed that the operative failure mode is the one associated with the smallest failure load.

4.1 Design variables

In this paper, the thickness of the skin, t_1, and the height of the orthogrid, d_r, the spacing between two orthogrid ribs, h, and the thickness of the rib, t_r, are set as variables while other parameters are fixed values. Diameter, D, is 625 mm and height, H, is 392.7 mm. The dimensionless design variables, X_i, are suggested as

$$\mathrm{X}=\left\{X_1,X_2,X_3,X_4\right\}^T=\left\{\frac{t_1}{D},\frac{d_r}{D},\frac{h}{D},\frac{t_r}{D}\right\}^T, \tag{40}$$

where $X_1=t_1/D$, denoting the dimensionless skin thickness; $X_2=d_r/D$, denoting

the dimensionless rib height; $X_3 = h / D$, denoting the dimensionless core thickness; $X_4 = t_r / D$, denoting the dimensionless rib thickness. The multi-failure criteria are

$$\frac{P_{cr1}}{\pi D^2 E_1} = \frac{2\beta\gamma}{\sqrt{3(1-\nu^2)}} X_1^{\ 2} \ , \gamma = 0.65, \tag{41}$$

$$\frac{P_{cr2}}{\pi D^2 E_1} = \frac{(1+\alpha+\mu) K_c \pi^2 D}{12(1-\nu^2) D} \frac{X_1^{\ 2}}{X_3^{\ 2}}, \tag{42}$$

$$\frac{P_{cr3}}{\pi D^2 E_1} = \frac{4(1+\alpha+\mu)\pi N_c \sqrt{D_1 D_2 + D_3}}{E_1 \eta D^3} \frac{X_1 X_3}{X_4 X_2^2}, \tag{43}$$

$$\frac{P_{cr4}}{\pi D^2 E_1} = \left[\frac{1}{X^2} \left(\frac{E_{r1}^2}{9} - \frac{2}{27} E_{r1} E_{r2} - \frac{E_{r2}^2}{27} \right) + \left(\frac{4}{9} \frac{E_{r2}}{Y} \right)^2 + \left(\frac{4}{3} \frac{G_{r12}}{S} \right)^2 \right]^{-\frac{1}{2}} (1+\alpha+\mu) X_1. \tag{44}$$

The failure load P_{cr} of the cylinder is the minimum one of the four failure loads as

$$P_{cr} = \min\{P_{cri}\} \text{ for } i = 1, 2, 3, 4. \tag{45}$$

4.2 Failure prediction with one variable

Failure mode maps of the sandwich cylinder based on load capacity are related to the variation of X_i, as shown in Fig. 6. X_1, X_2, X_3 and X_4 are dimensionless parameters, and in each map, there is only one variable while other three variables are constant, respectively. For the calculation in Fig. 6, constants of the fabricated sandwich cylinder were referenced in these predictions, where $t_1 = 1$ mm . $h = 327$ mm, $d_r = 8$ mm and $t_r = 4$ mm.

As shown in Fig. 6(a), only the variation of the dimensionless skin thickness was discussed. With the increase of skin thickness, the peak load increases. When $X_1 < 0.0006$, the dominated failure mode is monocell buckling, while it transfers to strength failure when $X_1 > 0.0006$. It means that cylinder with thick skins has a tendency to strength failure. Meanwhile, the other three failure modes show larger

load capacity which can't control the failure of the cylinder.

As shown in Fig. 6(b), only the variation of the dimensionless core thickness was discussed. Strength failure is the fatal failure mode. The other three failure modes always have larger load capacity no matter the value of X_2 in the calculation.

As shown in Fig. 6(c), only the variation of the dimensionless cell length was discussed. A peak value appears when $X_3 = 0.08$. If the cell length is small, load capacity of the cylinder will be dominated by strength failure. If the cell length is large, load capacity of the cylinder will be dominated by the monocell buckling.

As shown in Fig. 6(d), only the variation of the dimensionless parameter was discussed. Increasing the rib thickness will increase the load capacity of the cylinder. Initially, with thin rib, the cylinder will collapse at the mode of lattice buckling. A breaking point appears at $X_4 = 0.001$. After the point, with thicker rib, strength failure appears and slowly increases the load capacity of the cylinder.

In all the four figures, strength failure is the most common fatal failure modes.

4.3 Failure maps

These maps are developed as a function of two dimensionless parameters, including t_1 / D and d / D. The boundaries of each failure mode are obtained by evaluating the minimum P_{cr} at given values of some non-dimensional parameters while the others keep constant. The elastic modulus of upper and lower skin, E_1, E_2 are 25.4 GPa. The elastic modulus of the fiber in fiber direction, E_{r1}, is 58 GPa, and in vertical, E_{r2}, is 4.8 GPa. The shear modulus, G_{r12}, is 2.8 GPa. The strength in the 1 direction is 493 MPa, and in 2 direction is 10.44 MPa. The shear strength is 9.28 MPa, and the

Poisson's ratio is 1/3. The distribution of failure modes is given with different cell number, N_c, and width of the grid, t_r, as shown in Fig. 7.

When N_c=30 and $t_r = 2$ mm, the parameters are consistent with the actual test, it can be seen that area is divided into four regions, containing all the four failure modes mentioned. When the thickness of the skin is thin, it's easy to have skin wrinkling. When the skin thickness is thick, it's easy to have grid element buckling and strength failure. Strength failure is easy to occur with shorter height of grid, and grid element buckling is likely to occur when grid height is higher. Global buckling only accounts for a small part, because it needs two conditions for instability. One condition is the local stiffness is high, and the other is the height of grid is short. Then, it can be considered as global buckling of a thin-walled cylinder. However, the strength failure is under consideration. So, when the skin is thicker, it increases the stiffness of cylinder and the strength failure is prone to occur.

4.4 Discussions

Compared with the experimental results, the bearing capacity of the theoretical prediction is higher than the experimental value, but the failure mode of the theoretical prediction is in good agreement with the test results. This structure itself has the initial imperfection and material has instability in the preparation process, so there are many factors affecting the mechanical properties of orthogrid-core sandwich cylinder. Preparation of cylinder needs high quality requirements of precision molds and reasonable process scheme.

According to the actual situation, another prediction is given. The load capacity of

the cylinder, P_{cr5}, can be determined by a simple equation as [20]

$$P_{cr5} \approx 2\pi D t_1 E_s \varepsilon_{cr}, \tag{46}$$

where ε_{cr} is the average strain at failure. Usually $\varepsilon_{cr} \approx 3\times10^3 \sim 4\times10^3\ \mu\varepsilon$ from previous experiments [10, 11]. Dimensionless peak load is given by

$$\frac{P_{cr5}}{\pi D^2 E_s} \approx 2X_1 \varepsilon_{cr}, \tag{47}$$

According to the compression test, the average strain is ε_{cr}=3545 με [20] at peak load, Eq. (47) can consistently predict the peak load, as shown in Figs. 6 and 8.

5 Conclusions

In this paper, a smearing method was proposed to analyze the behaviors of the CFRC orthogrid sandwich cylinder. Based on this homogenization method, multi-failure criteria of the orthogrid sandwich cylinder was developed, including global buckling, skin wrinkling, grid element buckling and material strength failure.

The dimensionless analyses compared these four potential failure modes and reveal the geometrical conditions for the appearance of each failure. It is found in practical design range the material failure and the monocell buckling should be concerned more seriously, especially the material failure. The theory correctly predicts the failure mode in experiment. As the theory overestimates the ultimate load of the cylinder, an engineering method based on engineering permitted strain was suggested and this method is more consistent to the experiment.

Acknowledgments

Supports from National Natural Science Foundation of China (11372095, 11672130) are gratefully acknowledged.

References

[1] Fan HL, Zeng T, Fang DN, and et al. Mechanics of advanced fiber reinforced lattice composites. Acta Mech Sin 2010;26:825-35.

[2] Fan HL, Meng FH, Yang W. Mechanical behaviors and bending effects of carbon fiber reinforced lattice materials. Arch Appl Mech 2006;75:635-47.

[3] Liu JY, Xiang LL, Kan T. The effect of temperature on the bending properties and failure mechanism of composite truss core sandwich structures. Compos Part A 2015;79:146-54.

[4] Kim TD. Fabrication and testing of composite isogrid stiffened cylinder. Compos Struct 1999;45 (1):1-6.

[5] Vasiliev VV, Barynin VA, Razin AF. Anisogrid composite lattice structures – Development and aerospace applications. Compos Struct 2012;94:1117-1127.

[6] Vasiliev VV, Razin AF. Anisogrid composite lattice structures for spacecraft and aircraft applications. Compos Struct 2006;76:182-9.

[7] Morozov EV, Lopatin AV, Nesterov VA. Buckling analysis and design of anisogrid composite lattice conical shells. Compos Struct 2011;93: 3150-62.

[8] Totaro G. Local buckling modelling of isogrid and anisogrid lattice cylindrical shells with hexagonal cells. Compos Struct2013;95: 403-10.

[9] Wang D, Abdalla MM. Global and local buckling analysis of grid-stiffened composite panels. Compos Struct 2015;119:767-76.

[10] Fan HL, Fang DN, Chen LM, et al. Making and testing of a CFRC sandwich cylinder with Kagome cores. Compos Sci Tech 2009;69:2695-700.

[11] Chen LM, Sun FF, Zhao L, et al. Improved manufacturing method and mechanical performances of carbon fiber reinforced lattice-core sandwich cylinder. Thin wall Struct 2013;68:75-84.

[12] Fan HL, Meng FH, Yang W. Sandwich panels with Kagome lattice cores reinforced by carbon fibers. Compos Struct 2007;81:533-9.

[13] Fan HL, Yang L, Sun FF. Compression and bending performances of carbon fiber reinforced lattice core sandwich composites. Compos Part A 2013;52:118-25.

[14] Zhang H, Sun FF, Fan HL, et al. Free vibration behaviors of carbon fiber reinforced lattice-core sandwich cylinder. Compos Sci Technol 2014;100;26-33.

[15] Hu Y, Li WX, An XY, et al. Fabrication and mechanical behaviors of corrugated lattice truss composite sandwich panels. Compos Sci Tech 2016; 125: 114-22.

[16] Han YS, Wang P, Fan HL, et al. Free vibration of CFRC lattice-core sandwich cylinder with attached mass. Compos Sci Technol 2015;118:226-35.

[17] Li WX, Sun FF, Wang P, and et al. A novel carbon fiber reinforced lattice truss sandwich cylinder: Fabrication and experiments. Compos Part A 2016;81:313-22.

[18] Yang JS, Xiong J, Ma L, and et al. Modal response of all-composite corrugated sandwich cylindrical shells. Compos Sci Technol 2015;115:9-20.

[19] Sun FF, Fan HL, Zhou CW, et al. Equivalent analysis and failure prediction of quasi-isotropic composite sandwich cylinder with lattice core under uniaxial compression. Compos Struct 2013;101:180-90.

[20] Jiang S, Sun FF, Fan HL, and et al. Fabrication and testing of composite orthogrid sandwich cylinder. Compos Sci Tech 2017; 142: 171-9.

Figure captions

Fig. 1 Orthogrid-core sandwich cylinder [20].

Fig. 2 FEM simulated buckling failure modes of orthogrid-core sandwich cylinder.

Fig. 3 Equivalent process of (a) the orthogrid and (b) the orthogrid-core sandwich and (c) central coordinate of sandwich structure.

Fig. 4 Force diagram of orthogrid-core sandwich.

Fig. 5 Failure modes of orthogrid-core sandwich cylinder.

Fig. 6 Load capacity prediction of the sandwich cylinder related to the variation of (a) the skin thickness, (b) the dimensionless core thickness, (c) the dimensionless cell dimension and (d) the dimensionless rib thickness.

Fig. 7 Distribution of failure modes with different parameters for (a) N_c=30, t_r=2mm; (b) N_c=30, t_r =1mm; (c) N_c=30, t_r =4mm and (d) N_c=60, t_r =2mm.

Fig. 8 Failure map for cylinder with N_c=30 and t_r=2mm based on modified strength criterion.

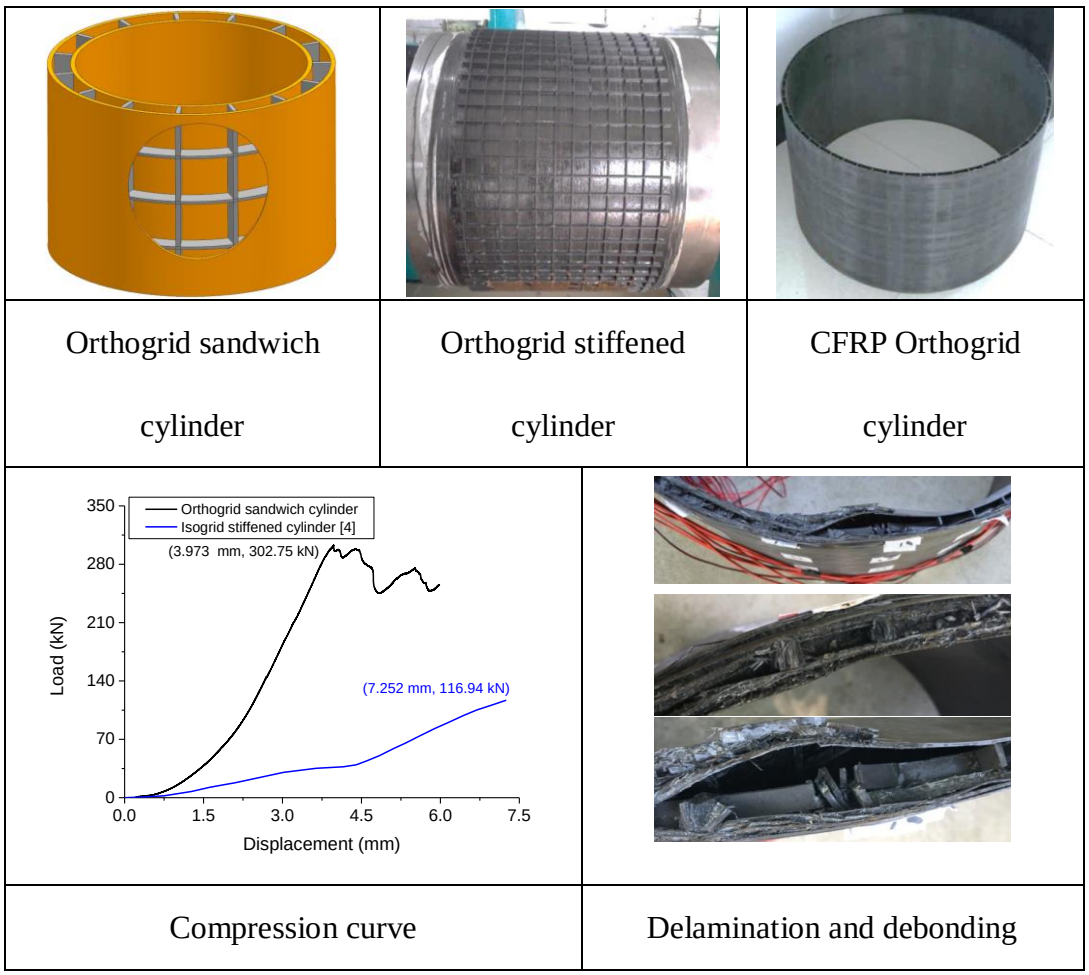

Fig. 1 Orthogrid-core sandwich cylinder [20]

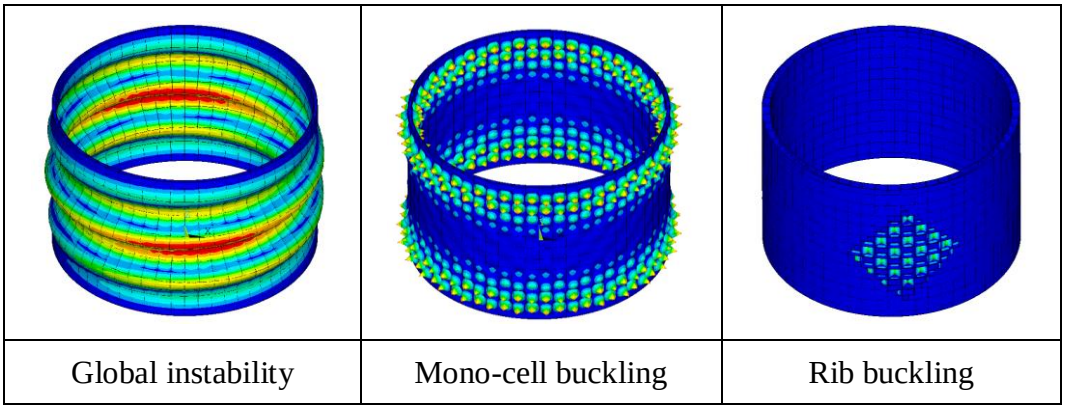

Fig. 2 FEM simulated buckling failure modes of orthogrid-core sandwich cylinder.

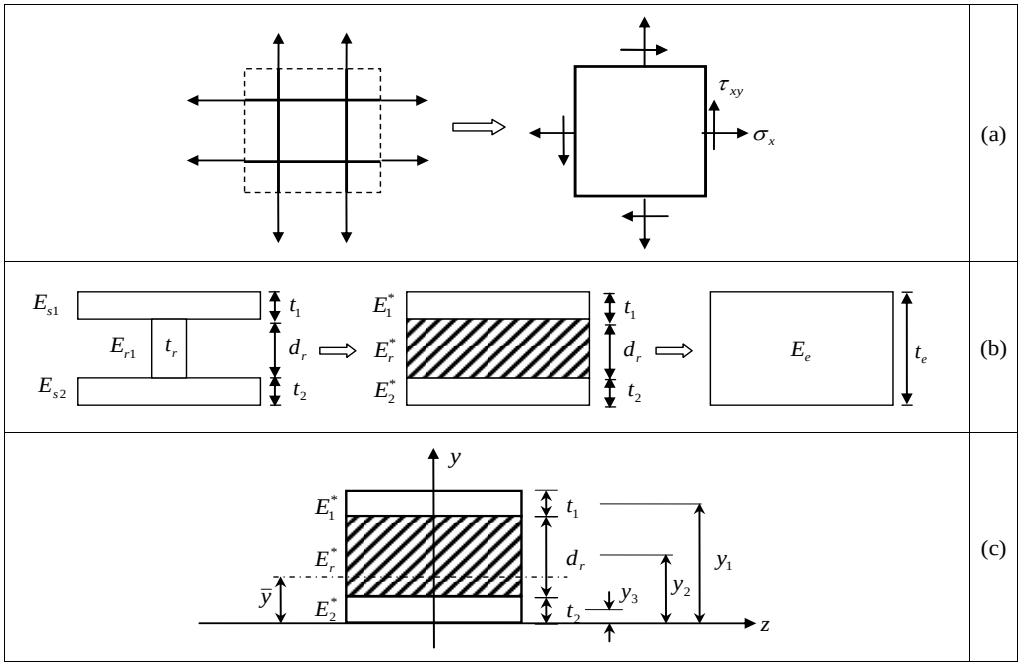

Fig. 3 Equivalent process of (a) the orthogrid and (b) the orthogrid-core sandwich and (c) central coordinate of sandwich structure.

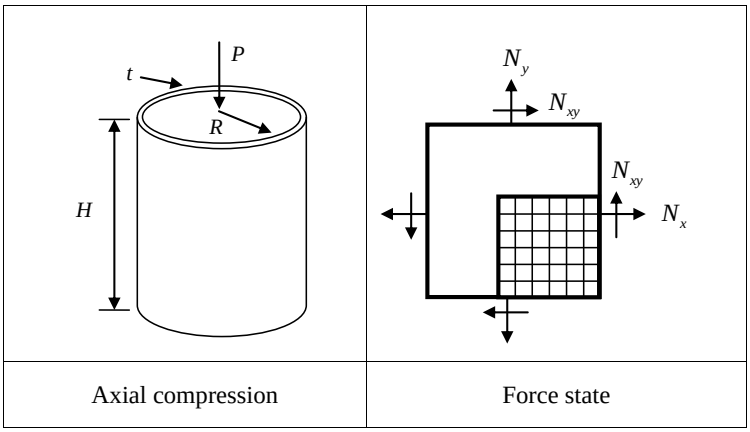

Fig. 4 Force diagram of orthogrid-core sandwich.

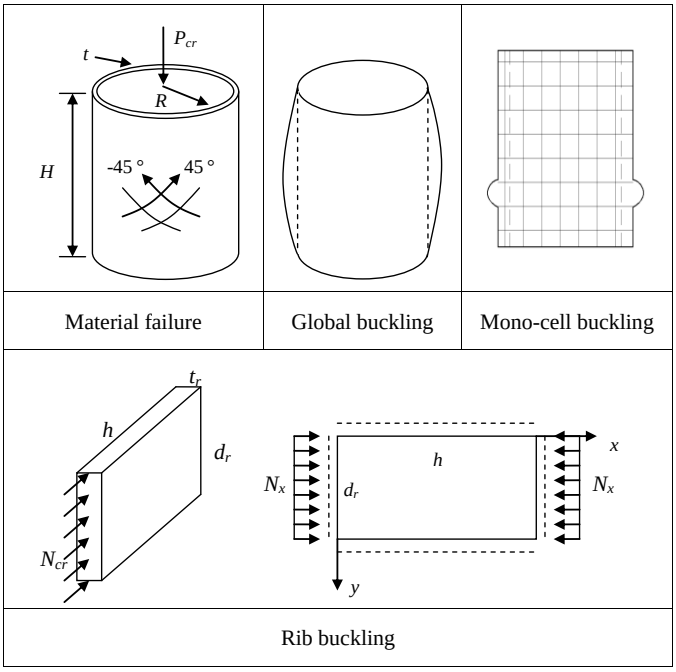

Fig. 5 Failure modes of orthogrid-core sandwich cylinder.

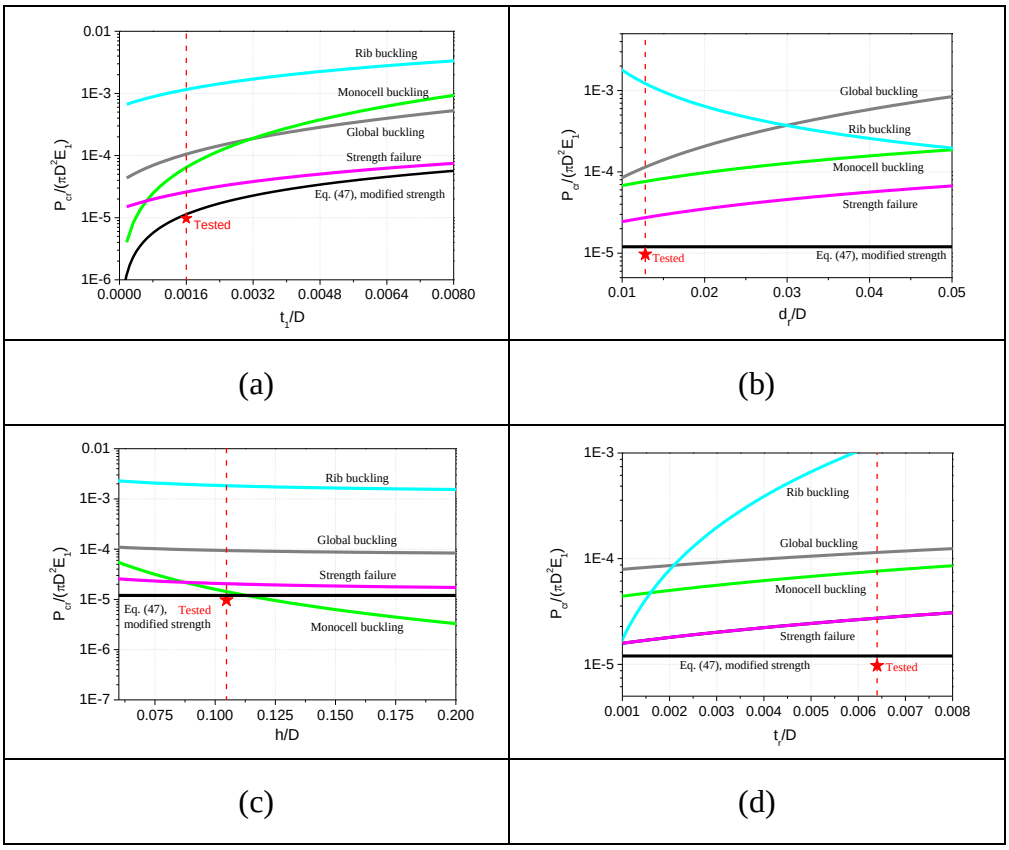

Fig. 6 Load capacity prediction of the sandwich cylinder related to the variation of (a) the skin thickness, (b) the dimensionless core thickness, (c) the dimensionless cell dimension and (d) the dimensionless rib thickness.

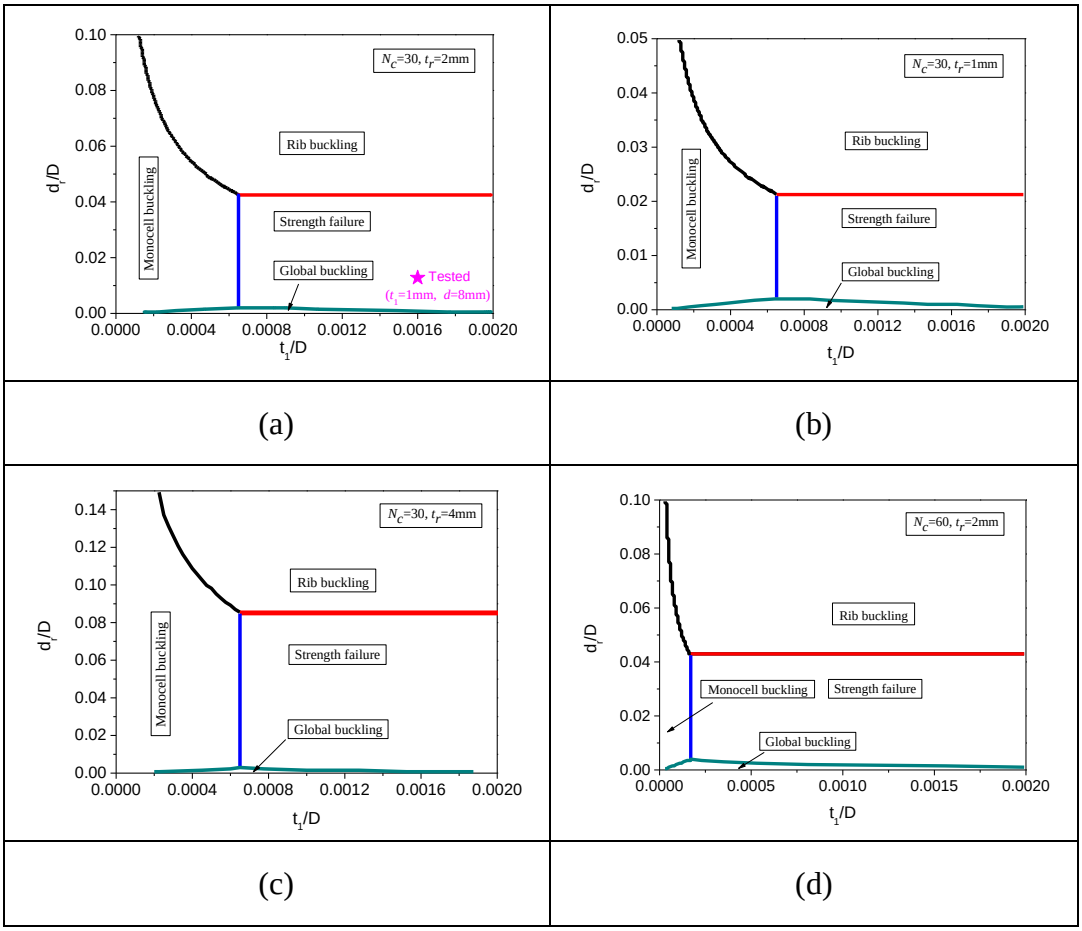

Fig. 7 Distribution of failure modes with different parameters for (a) N_c=30, t_r=2mm; (b) N_c=30, t_r =1mm; (c) N_c=30, t_r =4mm and (d) N_c=60, t_r =2mm.

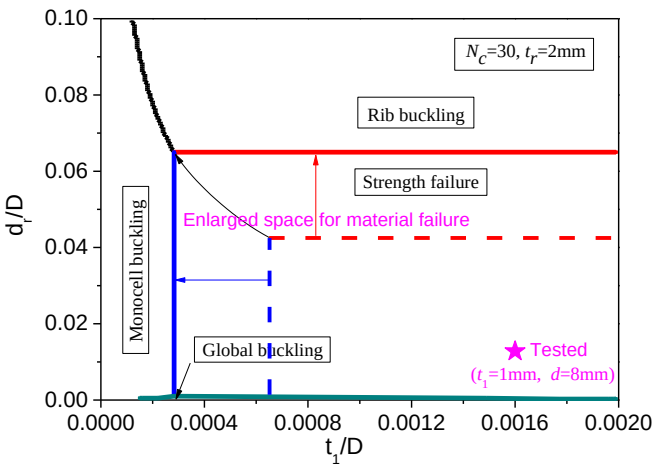

Fig. 8 Failure map for cylinder with N_c=30 and t_r=2mm based on modified strength criterion.